Thermoelectric properties of $Ca_{0.9}Yb_{0.1}MnO_{3-x}$ prepared by spark plasma sintering in air atmosphere

Jacques G. Noudem,[a,b,*] Simon Quetel-Weben,[a] Richard Retoux,[a] Geoffroy Chevallier[c] and Claude Estournès[c]

[a]*CRISMAT, UMR 6508 CNRS/ENSICAEN, 6 bd Maréchal Juin, 14050 Caen Cedex 4, France*
[b]*LUSAC, Université de Caen Basse-Normandie, rue Aragon 50130 Cherbourg, France*
[c]*Institut Carnot CIRIMAT, UMR 5085 CNRS 118, route de Narbonne, 31062 Toulouse Cedex 9, France*

In this paper we report the densification of $Ca_{0.9}Yb_{0.1}MnO_{3-x}$ ceramics by spark plasma sintering (SPS) in different atmospheres and using different tools. The thermoelectric properties of these ceramics are reported and compared to those of ceramics obtained by conventional sintering. This study clearly demonstrated the possibility for processing oxide materials by SPS under air atmosphere and overcomes the problem of reduction due to the low oxygen partial pressure (graphitic environment, dynamic vacuum or neutral atmosphere) commonly encountered.

Keywords: $Ca_{0.9}Yb_{0.1}MnO_{3-x}$; Spark plasma sintering; Air processing; Microstructure; Oxide thermoelectric properties

Since the introduction of spark plasma sintering (SPS) in laboratories, it has been clearly shown that this technique allows compact powders to be sintered into high-density materials at a relatively low temperature and shorter processing time compared to conventional sintering techniques [1–8]. Thus far, SPS has been applied to fabricate various types of materials [1–13]. It offers the possibility to accelerate the materials' densification and, in many cases, to control grain growth [14–18] with respect to other sintering methods [19,20]. In most of the SPS experiments reported, graphite tools and controlled environments (vacuum or inert atmosphere) are used, which lead to a low oxygen partial pressure inside the SPS chamber. Air sintering is sometimes essential for various oxide materials, such as the perovskite $Ca_{0.9}Yb_{0.1}MnO_{3-x}$ thermoelectric (TE) material investigated in this work. This compound is one of the few promising and most studied n-type oxide TE materials [21–23]. The TE properties of such materials are sensitive to oxygen deficiency due to the mixed valency of manganite (Mn^{3+}, Mn^{+4}) they present. In this study, dense $Ca_{0.9}Yb_{0.1}MnO_{3-x}$ ceramics were processed by SPS in air atmosphere using various tools. The structural and TE properties were investigated and found to differ significantly from those of materials obtained by normal SPS.

In previous works [23], we have published the processing details of the synthesis of manganite powder ceramic. Briefly, the nanosized $Ca_{0.9}Yb_{0.1}MnO_{3-x}$ powders were synthesized by the coprecipitation technique. Calcium carbonate ($CaCO_3$, 99.9%, Cerac), manganese carbonate ($MnCO_3$, 99.9%, Sigma-Aldrich) and ytterbium nitrate ($Yb(NO_3)_3.6H_2O$, 99.99%, Sigma-Aldrich) were first dissolved in dilute nitric acid with hydrogen peroxide promoter followed by adding distilled water to make it into nitrate stock solution. Ammonium carbonate was dissolved in distilled water, to serve as the precipitant solution. The coprecipitation commenced by adding the nitrate stock solution to the precipitant solution, with stirring. The resultant suspension was subjected to suction filtration. The filtration cake was washed with water before drying and calcined in air.

The final processing (sintering) was carried out either in a classical furnace or using the SPS system (Dr Sinter SPS 2080, Sumitomo Coal Mining Co. Ltd, Japan) of the Plate-forme Nationale CNRS de Frittage Flash (PNF2/CNRS) located at the University Paul Sabatier in Toulouse. The following samples have been processed:

* Corresponding author at: CRISMAT, UMR 6508 CNRS/ENSICAEN, 6 bd Maréchal Juin, 14050 Caen Cedex 4, France. Tel.: +33 231 45 13 66; fax: +33 231 45 13 09; e-mail: jacques.noudem@ensicaen.fr

(1) For the first sample (S1), green powder was mixed with the polyvinyl alcohol binder and pelletized (20 mm) under 100 MPa uniaxial pressure before being conventionally sintered at 1200 °C under air with a heating rate of 100 °C min^{-1} and a dwell time of 2 h.
(2) For the second sample (S2), the powder introduced in a graphite mold (diameter = 15 mm), covered with a graphite foil for easy removal of the densified pellet, was sintered by SPS at 900 °C using 100 °C min^{-1} and an applied pressure of 50 MPa, with a dwell time of 5 min under dynamic vacuum.
(3) For the third sample (S3), the powder is introduced into a tungsten carbide (WC) die (diameter = 15 mm) covered with a graphic foil, then placed into the working chamber in air atmosphere. The temperature was increased (100 °C min^{-1}) up to the chosen sintering value of 600 °C while a load of 94.2 kN (300 MPa) was applied for 20 min.
(4) For the fourth sample (S4), the powder was introduced in a steel tool (Inco718) covered with a graphite foil. The sample heating rate of 100 °C min^{-1} was used and the sample was densified in air at 700 °C, under 15.7 kN (50 MPa) with a dwell time of 20 min.

Basically, the samples processed by SPS even in air were annealed at 550 °C using the air atmosphere in order to remove the graphite foil used during processing before the polishing stage.

The valence state of Mn and oxygen content were determined by iodometric titration [24]. The samples were crushed and dissolved in sulfuric acid solution in an argon atmosphere to avoid the oxidation of any ion in solution. Basically, the valence state of manganese was determined from the chemical reaction between the Mohr salt $(NH_4)_2Fe(SO_4)_2{\cdot}6H_2O$ solution and potassium permanganate ($KMnO_4$) solution. The density of the compacted samples was determined by using Archimedes method (Kern & Sohn GmbH, Balingen, Germany); deionized water was used as a liquid medium.

Phase identification was achieved using an X'Pert powder diffractometer in Bragg–Brentano geometry. Microstructural analysis was performed on fracture surfaces containing the pressing axis during processing or faces perpendicular to the applied pressure by scanning electron microscopy (SEM) using a Carl Zeiss Supra 55 microscope (Oberkochen, Germany) in backscattering electron mode.

Bar-shaped samples of length 10 mm and cross-section $2 \times 2\ mm^2$ were cut from the processed samples using a low-speed diamond saw (Struers, Champigny sur Marne, France), for physical characterization. The TE properties were measured (steady-state from 25 to 600 °C) by the DC four-probe method using a ZEM-3thermoelectric power and electrical resistivity measuring system (ULVAC-RIKO Inc., Japan).

Room-temperature X-ray diffraction (XRD) patterns of the as-processed $Ca_{0.9}Yb_{0.1}MnO_3$ samples were performed. The diffraction peaks of all samples (S1, S2, S3 and S4) can be indexed based on the orthorhombic "parent" $CaMnO_3$ structure in space group *pnma* [25]. Lattice parameters were calculated. As seen in Table 1, the lattice parameters do not show any significant variation for S1, S3 and S4 samples. However, the *a*, *b* and *c* parameters are different for sample S2. This can be explained by the processing atmosphere used: vacuum in the case of sample S2 and air atmosphere for samples S1, S3 and S4. We can also notice that the cell volume of S2 is lower than for the other samples. This might be due to the low oxygen partial pressure atmosphere seen by this sample during the sintering cycle, which may induce the oxidation state of manganese and oxygen deficiency in the ceramic as titration seems to indicate different $Ca_{0.9}Yb_{0.1}MnO_{3-x}$ samples with $x = 0.01$, 0.21, 0 and 0.03 for S1, S2, S3 and S4, respectively.

The bulk densities are 4.70, 4.72, 4.64 and 3.99 g cm^{-3} for S1, S2, S3 and S4 samples, respectively, in comparison with the theoretical density of 4.99 g cm^{-3} calculated from XRD patterns. One can clearly note here the influence of the applied pressure and the temperature on the density of the materials.

Figure 1 shows SEM images from the fractured cross-sections of the samples S1, S2, S3 and S4. A typical SEM image of the starting CSM powder is shown in Figure 1a (insert). It clearly reveals that these powders are formed of spherical aggregates of very small crystallites. Moreover, these aggregates have uniform sizes (diameter of ~10 μm). These crystallites have well-defined shapes and are uniform in size with very narrow distributions of ~60–70 nm.

Contrary to what the Archimedes measurement indicates (Table 1), it can be clearly observed from SEM micrography on a fracture (Fig. 1a) that this sample is fully dense as few pores are visible. Tremendous grain growth occurred during its conventional sintering at 1200 °C for 2 h. The fracture of the sample seems to be intergranular.

SPS processing results in a homogeneous microstructure with narrow grain size distribution. As expected,

Table 1. Lattice parameters deduced from XRD refinement of $Ca_{0.9}Yb_{0.1}MnO_3$ samples processed by (S1) conventional sintering and SPS, and (S2) using graphite mold; and using (S3) tungsten carbide and (S4) steel tools.

Sample	Mold	Sintering conditions						Crystallographic parameters			
		T (°C)	Dwell time (min)	Applied pressure (MPa)	Atmosphere	Mass volumic (g cm^{-3})	Relative density	*a* (Å)	*b* (Å)	*c* (Å)	*V* (Å^3)
Powder								5.283	7.458	5.267	207.533
S1	Steel	1200	120	100	Air	4.70	94.2	5.296	7.466	5.268	208.300
S2	Graphite	900	5	50	Vacuum	4.72	94.5	5.303	7.514	5.192	206.570
S3	WC	600	20	300	Air	4.64	93	5.314	7.471	5.278	207.736
S4	Steel	700	20	50	Air	3.99	80	5.287	7.440	5.270	207.296

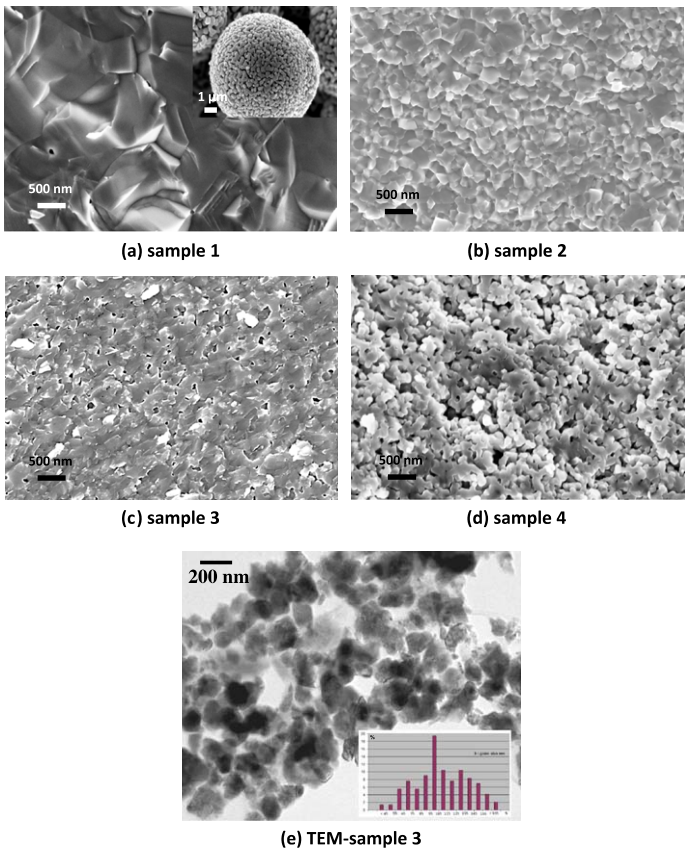

Figure 1. SEM micrographs of samples (a) S1, (b) S2, (c) S3 and (d) S4. TEM of sample S3 (e) and the grain size distribution (insert) are also shown.

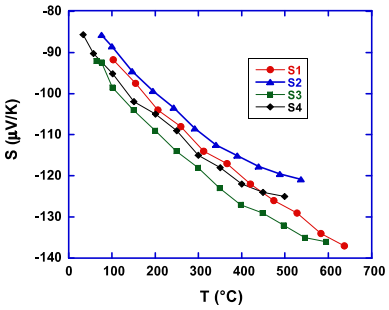

Figure 2a. Temperature dependence of thermopower for samples S1, S2, S3 and S4.

the sample (S2) consolidated by SPS from the graphite tool at 900 °C, 5 min seems to be dense with an average grain size of 200–300 nm (Fig. 1b). Here again the fracture seems to be intergranular. For sample S3, Figure 1c shows that, even though using the WC tool, which allows us to work under air and to apply high uniaxial pressure (300 MPa), 600 °C and a dwell time of 20 min are not enough to obtain a fully densified ceramic. The sample prepared by using the steel mold contains more pores (Fig. 1d) than other samples due to the low temperature and pressure applied during processing.

In order to confirm the average grain size of this air SPS sintered sample, transmission electron microscopy (TEM) observations have been undertaken on a crushed S3 sample. After dispersion of the crystallites in alcohol a drop of the suspension is deposited and dried onto a carbon-coated copper grid. The TEM observations were performed using a 200 kV JEOL 2010 FEG transmission electron microscope fitted with a double-tilt sample holder (tilts ±42°). The cationic composition of the crystallites was verified using energy-dispersive X-ray analysis (EDX) using an EDAX analyzer attached to the microscope. This analysis is in good agreement with the nominal composition. Figure 1e shows the typical grain size distribution and the improved homogeneity of these samples, while electron diffraction and EDX analysis performed on several crystallites confirmed their structure parameters and chemical formulation. This homogeneity of the grains is evidenced by the histogram (insert Fig. 1e), where 96% present a grain size between 45 and 165 nm.

The thermopower vs. temperature (Fig. 2a) relationship of the samples has been performed. All the samples show a negative-type Seebeck over the entire temperature range, indicating that electron conduction dominates the transport properties. The absolute value of thermopower increases with increasing temperature as compared to those reported elsewhere [26,27]. However, we can note that the Seebeck coefficient of S2 sample processed using a graphite tool under vacuum is lower than those of the samples prepared in air atmosphere. This difference can be attributed to the contribution of the oxygen deficiency, confirmed by the oxygen content analyses, as it is well known that sintering under vacuum (low oxygen partial pressure) is a reducing condition. To confirm that, redox titrations have been performed on the samples and allow us to propose the following chemical compositions: (i) $Ca_{0.9}Yb_{0.1}MnO_{2.99}$, (ii) $Ca_{0.9}Yb_{0.1}MnO_{2.79}$,

(iii) $Ca_{0.9}Yb_{0.1}MnO_{3.00}$ and (iv) $Ca_{0.9}Yb_{0.1}MnO_{2.97}$, respectively, for samples S1, S2, S3 and S4.

Figure 2b shows the temperature dependence of electrical resistivity (ρ) and power factor (*PF*). Several features can be clearly seen:

(1) The electrical resistivity (open symbols) of all samples shows the same semiconductor behavior over the whole range studied (75–600 °C). One can observe that the resistivity of the parent S1 sample, i.e. the conventionally sintered one, is lower than other samples. This seems to be caused by the decrease in the carrier density in the case of sample S2, and improvement of the grain boundaries and better densification as compared to samples S3 and S4.

(2) The *PF* (plain symbols) represents the electrical component of the TE performance. It is defined by $PF = S^2/\rho$, where S is the thermopower, i.e. the Seebeck value, and ρ is the electrical resistivity. It is obvious that *PF*, for all samples, increases with temperature. The values obtained at high temperature (~500 °C) are correlated to the microstructure and resistivity measurements. The *PF* values are 100 and 240 $\mu W\,m^{-1}\,K^{-2}$ at 550 °C for S2 and S3 samples prepared using graphite and tungsten carbide molds, respectively. The difference between the TE properties of the samples suggests as evidenced by redox titration that the oxygen stoichiometry plays an important role. The thermopower decreases with the oxygen deficiency, showing an increase in charge carriers due to the mixed valence of Mn^{4+} and Mn^{3+}. The *PF* of the sample (S3) processed (600 °C, in air) with the WC tool close to the reference sample (S1) is an interesting result. This demonstrates that by optimizing the processing conditions and using a suitable tool we can process TE oxide materials in air atmosphere by SPS.

In summary, this study clearly demonstrates that below 800 °C, it is possible to process the mixed-valence oxide materials in air by SPS. Using steel and a tungsten carbide tool, SPS enables the preparation in air of the TE $Ca_{0.9}Yb_{0.1}MnO_3$ ceramic with a small grain size. Structural analyses show that the samples were single phase with orthorhombic structure. The TE properties of the sample processed by SPS in air are comparable with those of material obtained by conventional sintering. This study offers the possibility to use SPS in air to densify the oxide material by choosing a suitable tool. Optimization of the properties is underway.

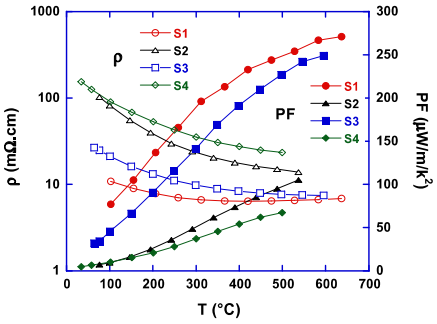

Figure 2b. Temperature dependence of electrical resistivity ρ (open symbols) and power factor *PF* (closed symbols) for all samples.

S.Q.-W. acknowledges a fellowship from the Ministère Français de la Recherche et de la Technologie. The authors thank the GDR-SPS (No. 3165) for support for the realization of this work.

[1] M. Tokita, Mater. Sci. Forum (2005) 711–718.
[2] R. Orrù, R. Licheri, A.M. Locci, A. Cincotti, G. Cao, Sci. Eng. R 63 (2009) 127.
[3] R. Chaim, M. Levin, A. Shlayer, C. Estournès, Adv. Appl. Ceram. 27 (2008) 159.
[4] M. Yue, J.X. Zhang, W.Q. Liu, G.P. Wang, J. Magn. Magn. Mater. 271 (2004) 367.
[5] M. Suganuma, Y. Kitagawa, S. Wada, N. Murayama, J. Am. Ceram. Soc. 86 (2003) 387.
[6] J.X. Zhang, Q.M. Lu, K.G. Liu, L. Zhang, M.L. Zhou, Mater. Lett. 58 (2004) 1981.
[7] Y. Liu, Y. Lin, Z. Shi, C.-W. Nan, Z. Shen, J. Am. Ceram. Soc. 88 (2005) 1337.
[8] Z.A. Munir, D.V. Quach, M. Ohyanagi, J. Am. Ceram. Soc. 94 (1) (2011) 1–19, ISBN 0027820.
[9] U.-Chan Chung, C. Elissalde, M. Maglione, C. Estournès, M. Paté, J.P. Ganne, Appl. Phys. Lett. 92 (2008) 042902.
[10] C. Estournès, D. Oquab, S. Selezneff, M. Boidot, D. Monceau, D. Grossin, C. Drouet, U.-Chan Chung, F. Roulland, C. Elissalde, M. Maglione, R. Chaim, Ph. Miele, J. Gurt-Santanach, G. Chevallier, A. Weibel, A. Peigney, Ch. Laurent, Mater. Sci. Forum 706–709 (2012) 24.
[11] J.G. Noudem, J. Eur. Ceram. Soc. 29 (2009) 2659.
[12] J.G. Noudem, D. Kenfaui, S. Quetel-Weben, C.S. Sanmathi, R. Retoux, M. Gomina, J. Am. Ceram. Soc. 94 (2011) 2608.
[13] J.G. Noudem, D. Kenfaui, D. Chateigner, M. Gomina, Scr. Mater. 66 (2012) 258.
[14] Tomonari Takeuchi, Mitsuharu Tabuchi, Hiroyuki Kageyama, Yoko Suyama, J. Am. Ceram. Soc. 82 (1999) 939.
[15] T. Wada, K. Tsuji, T. Saito, Y. Matsuo, Jpn. J. Appl. Phys. 42 (2003) 6110.
[16] T. Hungria, J. Galy, A. Castro, Adv. Eng. Mater. 11 (2009) 615.
[17] Kazuyuki Kakegawa, Yukiko Kawai, Wu YongJun, Naofumi Uekawa, Yoshinori Sasaki, J. Am. Ceram. Soc. 87 (2004) 541.
[18] Rachel Marder, Rachman Chaim, Claude Estournès, Mater. Sci. Eng. A 527 (2010) 1577.
[19] H. Takahashi, Y. Numamoto, J. Tani, S. Tsurekawa, Jpn. J. Appl. Phys. 47 (2008) 8468.
[20] T. Karaki, K. Yan, T. Miyamoto, M. Adachi, Jpn. J. Appl. Phys. 46 (2007) L97.
[21] T. Kobayashi, H. Takizawa, T. Endo, T. Sato, H. Taguchi, M. Nagao, J. Solid State Chem. 92 (1991) 116.
[22] A. Maignan, C. Martin, B. Raveau, Mater. Res. Bull. 34 (1999) 345.
[23] C.S. Sanmathi, Y. Takahashi, D. Sawaki, Y. Klein, R. Retoux, I. Terasaki, J.G. Noudem, Mater. Res. Bull. 45 (2010) 558.
[24] M. Karppinen, A. Fukuoka, L. Niinisto, H. Yamauchi, Supercond. Sci. Technol. 9 (1996) 121.
[25] K.R. Poeppelmeier, M.E. Leonowicz, J.C. Scanlon, J.M. Longo, W.B. Yelon, J. Solid State Chem. 45 (1982) 71.
[26] Chia-Jyi Liu, Ankam Bhaskar, J.J. Yuan, Appl. Phys. Lett. 98 (2011) 214101.
[27] M. Ohtaki, H. Koga, T. Tokunaga, K. Eguchi, H. Arai, J. Solid State Chem. 120 (1995) 105.